

# Catalysis Science & Technology

Accepted Manuscript



This is an *Accepted Manuscript*, which has been through the Royal Society of Chemistry peer review process and has been accepted for publication.

*Accepted Manuscripts* are published online shortly after acceptance, before technical editing, formatting and proof reading. Using this free service, authors can make their results available to the community, in citable form, before we publish the edited article. We will replace this *Accepted Manuscript* with the edited and formatted *Advance Article* as soon as it is available.

You can find more information about *Accepted Manuscripts* in the [Information for Authors](#).

Please note that technical editing may introduce minor changes to the text and/or graphics, which may alter content. The journal's standard [Terms & Conditions](#) and the [Ethical guidelines](#) still apply. In no event shall the Royal Society of Chemistry be held responsible for any errors or omissions in this *Accepted Manuscript* or any consequences arising from the use of any information it contains.



Journal Name

ARTICLE

## Reactivity and Mechanism Investigation for Selective Hydrogenation of 2,3,5-Trimethylbenzoquinone on *in-situ* Generated Metallic Cobalt

Received 00th January 20xx,  
Accepted 00th January 20xx

DOI: 10.1039/x0xx00000x

www.rsc.org/

Diefeng Su,<sup>a,†</sup> Zhongzhe Wei,<sup>a,†</sup> Shanjun Mao,<sup>a</sup> Jing Wang,<sup>a</sup> Yi Li,<sup>a</sup> Haoran Li,<sup>a</sup> Zhirong Chen,<sup>a</sup> Yong Wang\*<sup>a</sup>

Efficient and inexpensive catalysts are urgently desired for the hydrogenation of 2,3,5-trimethylbenzoquinone (TMBQ) to 2,3,5-trimethylhydroquinone (TMHQ), a key Vitamin-E intermediate. In this study, a one-step method was developed to synthesize uniform cobalt-based NPs supported on porous nitrogen-doped carbon for the hydrogenation of TMBQ to TMHQ. The as-prepared catalyst shows high yield (> 90 %) and selectivity (> 99 %) for TMBQ hydrogenation as well as  $\alpha$ ,  $\beta$ -unsaturated carbonyls. The satisfactory performance is attributed to the small particle size and homogeneous distribution. Meanwhile, the metallic Co is proved to be responsible for the catalytic activity. Furthermore, the density functional theory calculation discloses that the excellent chemoselectivity towards TMBQ is due to the preference of desorption process to sequential hydrogenation of TMHQ. This novel material has great potential for heterogeneous hydrogenation process as non-precious-metal catalyst, relying on the outstanding catalytic performance, simple preparation method and low production cost.

### Introduction

Chemoselective hydrogenation represents one of the most important catalytic methodologies in synthetic organic chemistry, both on laboratory- and industrial-scale to produce fine chemicals, pharmaceuticals and functional materials.<sup>1-6</sup> Compared with homogeneous catalysis, heterogeneous catalysis plays a dominant role in synthesis of chemical products in industry due to the beneficial stability and recycling capability of the catalysts.<sup>7,8</sup> Hydrogen, notwithstanding its current mostly fossil-based production route, is always the preferred choice as an environmentally benign and clean reductant from an atom economy perspective. Up to now, precious metal-based materials, despite their high price and low abundance, are still considered as state-of-the-art hydrogenation catalysts because of their excellent activity and durability.<sup>9-11</sup> Thus, it is of great challenge to develop low-cost and highly efficient catalysts.

In this respect, we focus on the heterogeneous catalytic hydrogenation of 2,3,5-trimethylbenzoquinone (TMBQ) to 2,3,5-trimethylhydroquinone (TMHQ), a key intermediate step in the synthesis of Vitamin-E (VE).<sup>12,13</sup> A traditional way to prepare TMHQ is by means of chemical reduction with

reducing agents such as sodium thiosulfate. However, it is difficult to handle the tough problems such as high cost of reducing reagent, low yield and a great deal of sewage produced during the manufacturing process.<sup>14</sup> Consequently, catalytic hydrogenation with merits of good yield, environmental friendliness and recycling capability of the catalysts, has been considered as a better choice for the industrial-scale production of TMHQ.<sup>15</sup> The heterogeneous catalysts for such a reaction are dominated by noble metals.<sup>16,17</sup> Although the reported catalysts showed high activity for such a reaction, they are significantly more expensive. Recent years have witnessed an increasing interest in exploring and utilizing non-noble catalysts, e.g. iron- or cobalt-based materials, as promising alternatives to precious metal catalysts.<sup>18-20</sup> In particular, tremendous effort has been made on cobalt-based materials, which show great potential for Fischer–Tropsch synthesis, and partial oxidation of olefins.<sup>21-23</sup> Very recently, nanostructure cobalt oxide has been reported for the efficient and selective reduction of nitroarenes to anilines.<sup>24</sup> Therefore, it was expected that well-designed cobalt-based materials might also function as catalysts for heterogeneous hydrogenation of TMBQ.

It is well recognized that the catalyst particle size and dispersity, which are highly associated with catalytic activity, can be modified by introducing specific supports.<sup>25-27</sup> In the past few decades, carbon materials with unique electronic properties, large specific surface area and well-developed

<sup>a</sup> Department of Chemistry, Zhejiang University, Hangzhou 310028, P. R. China.  
E-mail Address: [chemwy@zju.edu.cn](mailto:chemwy@zju.edu.cn)

<sup>†</sup>These authors contributed equally to this work.

<sup>†</sup>Electronic Supplementary Information (ESI) available: Catalysts preparation method, characterizations of samples and DFT calculation results. See DOI: 10.1039/x0xx00000x

porosity have been widely investigated as catalytic supports.<sup>28,29</sup> Generally, large specific surface area is beneficial for the distribution of nanoparticles. Additionally, nitrogen-doped carbon materials exhibit great potential as novel supports because of the relatively small particle size and good dispersity of metal particles along with the decrease of metal leaching, which could be explained by the strong interaction between metal nanoparticles and nitrogen atom.<sup>30,31</sup> On the other hand, a mountain of work has reported various synthetic methods such as impregnation, sol-gel, hydrothermal *et al.* to prepare cobalt based catalysts.<sup>32-35</sup> Although great progress has been made, it is still a grand challenge to synthesize well-dispersed Co-based catalysts of optimal size via simple, low-cost and scalable methods. Fortunately, the special properties of nitrogen-doped porous carbon materials gave us opportunities to develop such Co-based catalysts with high activity and stability for heterogeneous hydrogenation.

As mentioned above, the chemoselective hydrogenation of TMBQ played an important role in industrial production where a slight improvement could reduce the production cost significantly. For this reaction, many researchers focused on the technological conditions, whereas little attention was paid on studying the mechanism of the hydrogenation of TMBQ. Hence it is undoubtedly essential to address this issue, which does not only offer guidance on the development of novel efficient catalysts, but also initiates a new direction for academic research. Recently, the density functional theory (DFT) calculation has been investigated worldwide to reveal the mechanism of catalytic process.<sup>36,37</sup> In the present work, we studied the TMBQ adsorption as well as the addition of the first and second H adatom at different carbon and oxygen positions of the benzoquinonoid ring by DFT calculations.

Herein, we successfully developed a novel method to fabricate uniform Co-based NPs supported on porous, nitrogen-doped carbon (denoted as CoO<sub>x</sub>@CN) via simple and efficient thermal condensation of inexpensive starting materials. Notably, the CoO<sub>x</sub>@CN catalyst was easily obtained through one-step thermal condensation of cheap and available starting materials, and the synthetic method was capable of scale-up production for practical applications. The as-prepared materials displayed excellent performance for the conversion from TMBQ to TMHQ. Moreover, the catalyst showed significantly high activity and selectivity towards  $\alpha$ ,  $\beta$ -unsaturated carbonyls. Detailed catalytic and physical studies demonstrated that metallic Co (denoted as Co<sup>0</sup>) was the active site for the hydrogenation of TMBQ. The DFT calculation was further utilized to study the TMBQ hydrogenation process on Co (1 1 1) surface and explain the excellent chemoselectivity towards TMHQ due to the favorable desorption process rather than sequential hydrogenation of TMHQ.

## Experimental

### Materials and Catalysts Preparation

D-glucosamine hydrochloride (GAH), melamine, glucose, Co(NO<sub>3</sub>)<sub>2</sub>•6H<sub>2</sub>O, Co(CH<sub>3</sub>COO)<sub>2</sub>•4H<sub>2</sub>O, CoSO<sub>4</sub>•7H<sub>2</sub>O, Cobalt powder and Co<sub>3</sub>O<sub>4</sub> were purchased from Aladdin. Unless

otherwise stated, all solvents and chemicals were used as delivered without further treatment. All gases (H<sub>2</sub>, N<sub>2</sub>) used for catalyst preparation and hydrogenation reaction were high purity.

The CoO<sub>x</sub>@CN catalyst was prepared by thermal condensation of D-glucosamine hydrochloride (GAH), melamine (MEL), and Co(Ac)<sub>2</sub>•4H<sub>2</sub>O at 900 °C in an inert flow. For comparisons, GAH/MEL, Co(Ac)<sub>2</sub>/MEL, Co(Ac)<sub>2</sub>/GAH, Co(Ac)<sub>2</sub>/glucose/ MEL were pyrolyzed under the same process and the obtained materials were named as CN, CoO<sub>x</sub>@M, CoO<sub>x</sub>@G and CoO<sub>x</sub>@GL, respectively. Similarly, the materials synthesized at different temperature were denoted as CoO<sub>x</sub>@CN-800, CoO<sub>x</sub>@CN-1000. The materials of CoO<sub>x</sub>@NCNTs, and CoO<sub>x</sub>@CN-S were fabricated through the same conditions as CoO<sub>x</sub>@CN except the different cobalt source. The AT-CoO<sub>x</sub>@CN catalysts were acquired by acid treatment of CoO<sub>x</sub>@CN with 2M HCl solution for 3 days at 50 °C. Co<sub>3</sub>O<sub>4</sub>/SiO<sub>2</sub>, Co<sub>3</sub>O<sub>4</sub>/ZrO<sub>2</sub> and Co<sub>3</sub>O<sub>4</sub>/TiO<sub>2</sub> were all obtained by impregnation method. Detailed synthetic process could be found in the support information.

### Characterization

Transmission electron microscope (TEM, Hitachi H7700), HRTEM, STEM-HAADF and STEM-EDX (Tecnai G2 F30 S-Twin) were applied to observe the morphology and particle size distribution, element distribution of the catalysts. Powder X-ray diffraction (XRD) patterns were measured on a D/tex-Ultima TV wide angle X-ray diffractometer equipped with Cu K $\alpha$  radiation (1.54 Å) to study the catalyst structure. The X-ray photoelectron spectra (XPS) were operated on an ESCALAB MARK II spherical analyzer using an aluminum anode (Al 1486.6 eV) X-ray source. The Raman spectra were collected on a Raman spectrometer (JY, HR 800) using 514-nm laser. Nitrogen adsorption analysis was performed at 77 K using a Micromeritics ASAP 2020 to investigate the surface areas and pore size distributions. The specific surface area was calculated based on Brunauer-Emmett-Teller (BET) method. Total pore volumes (V<sub>total</sub>) were calculated from the amount of nitrogen adsorbed at a relative pressure, P/P<sub>0</sub> of 0.97. The pore size distribution (PSD) plot was recorded according to DFT model. The Co and N contents were measured by atomic absorption spectrometry (AAS) and Vario El elemental analyzer (Element Analysis), respectively.

### Catalytic Test

The hydrogenation reactions were carried out in a 50 mL stainless-steel autoclave with an external temperature and stirring controller. In a typical experiment, the autoclave was filled with 1 g 2,3,5-trimethylbenzoquinone, 20 mg cobalt catalyst (CoO<sub>x</sub>@CN, 1.6 mmol %) and 15 mL isopropanol as solvent. The reactor was charged with H<sub>2</sub> to remove the air for 3 times and then sealed tight and pressurized to 2 MPa H<sub>2</sub>. The autoclave was placed into an oil-bath with magnetic stirring and the reaction started when the temperature reached at 100 °C. After the reaction, the reactor was cooled to room temperature and the product was collected to be analyzed on GC (Shimadzu, GC-2014) equipped with a Rtx-1071 column. The products

were further identified by GC-MS (Agilent Technologies, GC 6890N, MS 5970). For recycling test, 0.5 g 2,3,5-trimethylbenzoquinone, 20 mg cobalt catalyst (AT-CoO<sub>x</sub>@CN, 1.1 mmol %) and 7.5 mL isopropanol were added into the autoclave. Then the reaction was carried out under the same procedure. After reaction, the catalyst was collected after centrifugation and was washed with ethanol. The catalyst was dried in the vacuum oven at 40 °C overnight after washing 3 times. The dried catalyst was then used for the next run without any reactivation or purification.

### DFT Calculations

The calculations reported here were performed using periodic, spin-polarized DFT as implemented in Vienna ab initio program package (VASP).<sup>38,39</sup> The electron-ion interactions are described by the projector augmented wave (PAW) method proposed by Blöchl<sup>40</sup> and implemented by Kresse<sup>41</sup>. RPBE functional is used as exchange-correlation functional approximation and a plane wave basis set with an energy cutoff of 400 eV is used.<sup>42</sup> Only gamma point is used for the Brillouin zone sampling in the whole calculation process. The k-point mesh tests are shown in Table S1 in the supporting information. Co (1 1 1) surface was modeled with p (5×5) supercell containing a four-layer slab with 100 atoms. The periodic condition is employed along the x and y direction. The vacuum space along the z direction was set to be 13 Å. The upper two layer atoms in the cell are allowed to relax during the structure optimization and the bottom two layer atoms are fixed. The structure optimization is converged to < 0.02 eV and activation barrier is converged to < 0.05 eV. The reaction pathway and barriers were calculated by using the climbing image nudged elastic band (CI-NEB) method.<sup>43</sup>

The adsorption energy for TMBQ is defined as:

$$E_{\text{ads}} = E_{\text{tot}} - E_{\text{slab}} - E_{\text{TMBQ}}$$

Where  $E_{\text{tot}}$  is the total energy of TMBQ and catalyst with certain configuration;  $E_{\text{slab}}$  is the energy of the clean catalyst alone;  $E_{\text{TMBQ}}$  is the energy of TMBQ in the gas phase.

## Results and discussion

### Materials Characterization

Figure 1 illustrated the representative morphology, structure, and composition of the material CoO<sub>x</sub>@CN, which was calcined at 900 °C in an inert flow. During the material preparation, D-glucosamine hydrochloride, a biomass downstream product, was chosen as both the carbon and the nitrogen sources; Melamine served as the soft template for the temporary in-situ synthesis of porous graphitic carbon.<sup>44</sup> As shown in Figure 1, the cobalt based NPs are uniformly dispersed over the porous carbon matrix, demonstrating the excellent bonding between NPs and porous carbon. According to the particle size distribution (Fig. 1a), the average diameter of the Co based NPs is approximately 9 nm. The elemental mapping images (Fig. 1d) illustrated that the elements (C, N, O) are evenly distributed in the whole skeletal framework, which implied the doped hetero atoms in the carbon matrix might

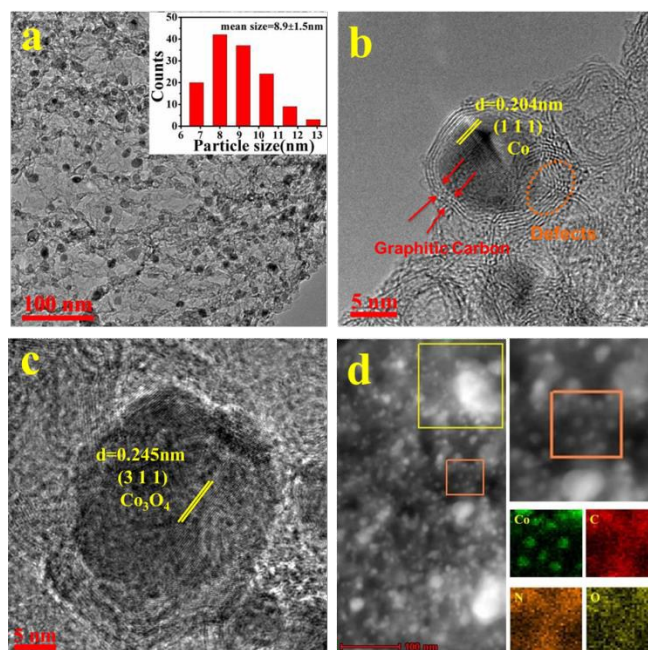


**Figure 1.** Representative TEM image (a), HRTEM images (b, c), STEM image and EDX elemental mapping (d) of CoO<sub>x</sub>@CN. Inset (a) is metal particle size distribution histogram of CoO<sub>x</sub>@CN.

prevent nanoparticles from agglomerating. The presence of cobalt oxide and metallic cobalt was corroborated by the HRTEM (Fig. 1b & 1c) images, demonstrating that the interplanar distances of cobalt oxide and metallic cobalt are 0.245 and 0.204 nm, respectively. In addition, a large number of Co species were covered by carbonaceous layers as illustrated in Fig. 1b. Moreover, the defects on the outside carbon layers were observed. The defects allowed the reactant to contact with internal metal nanoparticles so that the hydrogenation reaction could proceed efficiently.

The X-ray diffraction peaks of the CoO<sub>x</sub>@CN (Fig. 2a) are in good agreement with the face-centered cubic Co<sub>3</sub>O<sub>4</sub> configuration (JCPDS No.42-1467) and face-centered cubic Co (JCPDS No.15-0806), further confirming the coexistence of the Co<sub>3</sub>O<sub>4</sub> and Co phases. Moreover, the broad diffraction peaks may result from the small particle size of the cobalt based NPs. According to Scherrer equation, the equivalent particle sizes of Co<sub>3</sub>O<sub>4</sub> and Co in CoO<sub>x</sub>@CN are calculated to be 10 and 14.4 nm, respectively, which were calculated on the Co<sub>3</sub>O<sub>4</sub> (3 1 1) and Co (1 1 1) plane by Scherrer equation, being in line with the results of particle size distribution. In addition to XRD analysis, Raman measurement (Fig. 2b) provided extra strong evidence for the formation of Co<sub>3</sub>O<sub>4</sub> phase. The peaks detected at 190, 470, 510, 605 and 676 cm<sup>-1</sup> were assigned to the typical Raman-active modes (A<sub>1g</sub>, E<sub>g</sub> and 3F<sub>2g</sub>) of Co<sub>3</sub>O<sub>4</sub>.<sup>45</sup> Interestingly, all these five peaks were recorded with evident Raman shift, which possibly stemmed from the combined effects of strain and phonon confinement, indicating that the Co<sub>3</sub>O<sub>4</sub> particles were much smaller than the commercial Co<sub>3</sub>O<sub>4</sub>.<sup>46</sup> The existence of G (1590 cm<sup>-1</sup>) and D (1350 cm<sup>-1</sup>) bands unarguably declared the dual amorphous and crystalline nature of the carbonaceous matrix obtained herein.<sup>47</sup>

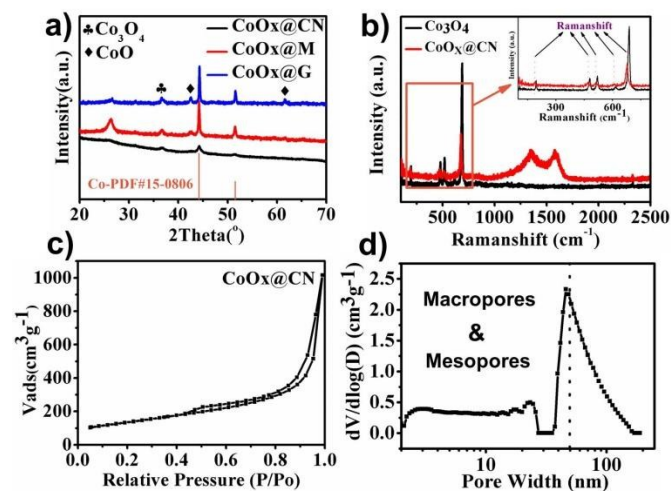


**Figure 2.** (a) XRD patterns of CoO<sub>x</sub>@CN; (b) Raman spectrum of commercial Co<sub>3</sub>O<sub>4</sub> and CoO<sub>x</sub>@CN; (c) Adsorption/desorption isotherms of CoO<sub>x</sub>@CN; (d) DFT pore size distribution of CoO<sub>x</sub>@CN.

The textural structure of CoO<sub>x</sub>@CN was investigated by N<sub>2</sub> sorption isotherms and pore size distributions (PSD) (Fig. 2d). N<sub>2</sub> adsorption-desorption isotherm curves with a pronounced hysteresis at relative pressure ( $p/p_0$ ) 0.4-0.6 indicate the existence of mesopore structures. Besides mesopores, the macropores are also evidenced by the sharp rise at  $p/p_0$  0.9-1.0. Judging from the DFT PSD, the mesopore and macropore structure was further confirmed. In general, hierarchically porous supports were deemed to reduce diffusion restriction to facilitate the mass transfer during reaction process.<sup>48,49</sup> On the other hand, the specific surface area was calculated to be 484 m<sup>2</sup> g<sup>-1</sup>, which again afforded plenty of active sites.

### Impacts on the Morphology and Structure of CoO<sub>x</sub>@CN

Then the influence of the carbon source GAH and soft template melamine on the morphology and structure of the final material was investigated. TEM images of the CoO<sub>x</sub>@M, CoO<sub>x</sub>@G and CoO<sub>x</sub>@CN materials demonstrated that the agglomerate phenomena were observed in both CoO<sub>x</sub>@M and CoO<sub>x</sub>@G (Fig. S1a, S1b), but uniform Co-based nanoparticles emerged in CoO<sub>x</sub>@CN (Fig. 1a). The uniform distribution of CoO<sub>x</sub>@CN implied that the soft template improved the dispersity of nanoparticles in precursor and the *in-situ* generated porous nitrogen-doped carbon matrix prevented nanoparticles from migrating and growing larger via the interaction between nanoparticles and carbon support. In addition, previous reports and above characterization indicated the doped N would impede the agglomeration of the metal NPs while particle size plays an important role in heterogeneous catalysis.<sup>29,48</sup> Thus, the N content of the three materials was measured by Element Analysis (Fig. S1d). As a result, the N content of CoO<sub>x</sub>@CN is as almost two times as that of CoO<sub>x</sub>@M and CoO<sub>x</sub>@G. Moreover, N<sub>2</sub> sorption isotherms analysis revealed the specific surface area and pore volume of CoO<sub>x</sub>@CN are the largest among the three materials (Fig. S1c, Table S2). Consequently, the components of GAH and melamine, which served as carbon & nitrogen sources respectively, are indispensable to the

production of CoO<sub>x</sub>@CN with small particle size and homogeneous distribution, relatively large specific surface area and rich nitrogen content.

Besides, cobalt source is also highly associated with particle size and morphology. TEM characterization (Fig. S2) discloses that the CoO<sub>x</sub>@CN possesses the smallest particle size in comparison with CoO<sub>x</sub>@NCNTs and CoO<sub>x</sub>@CN-S. It is supposed that the acetate would partially decompose and form carbon layers around the metal grains during the thermal condensation. The outside carbon layers further prevent the metal grains from agglomerating during the soft template underwent decomposition above 600 °C. To some extent, the carbon layers also cover active sites to catalyze the growth of carbon nanotube. As illustrated in TEM images of CoO<sub>x</sub>@CN, the flake-like carbon still exists in large scale when the temperature increases from 800 °C to 900 °C (Fig. S3a & Fig. 1a). However, a wide range of carbon nanotube appears in sample of CoO<sub>x</sub>@NCNTs (cobalt nitrate as cobalt source), when the temperature reaches 900 °C.<sup>24,50</sup> Apart from the particle size and morphology, the specific surface area could be adjusted by diverse cobalt source. As shown in Table S2, the specific surface area of the CoO<sub>x</sub>@CN material is the biggest one, which could be explained by the activation of carbon dioxide or carbon oxide resulting from the pyrolysis of carboxyl group. With these surprising findings, it could be expected that CoO<sub>x</sub>@CN materials might display excellent catalytic performance towards heterogeneous hydrogenation.

### Screening Catalysts for Hydrogenation of TMBQ

Next, the catalytic behavior of the different cobalt-based materials was tested. As summarized in Table 1 (Entry 1-3), the CoO<sub>x</sub>@CN catalyst performs better than CoO<sub>x</sub>@M and CoO<sub>x</sub>@G. XRD measurement indicates all those three samples consist of Co<sub>3</sub>O<sub>4</sub> and metallic Co (Fig. 2a). It is demonstrated that the particle size of CoO<sub>x</sub>@CN is much smaller than the other two in TEM characterization (Fig. S1). Similarly, the catalytic activity of CoO<sub>x</sub>@CN, CoO<sub>x</sub>@NCNTs, and CoO<sub>x</sub>@CN-S successively decrease with the increase of the particle size of the corresponding materials (Fig. S2). In addition, the introduction of hetero atoms would also benefit for the improvement of the hydrogenation activity, especially nitrogen.<sup>51</sup> To shed light on this point, the CoO<sub>x</sub>@GL catalyst was evaluated, showing inferior activity in comparison with CoO<sub>x</sub>@CN (Table 1, Entry 4). Higher nitrogen content is possibly ascribed to the better catalytic activity, because there is no obvious difference between CoO<sub>x</sub>@GL and CoO<sub>x</sub>@CN catalysts based on XRD and BET analyses except nitrogen content (Fig. S4). As a result, the CoO<sub>x</sub>@CN material was eventually chosen as the optimized catalyst for the hydrogenation of TMBQ. What is more, the CoO<sub>x</sub>@CN catalyst also shows high activity and excellent selectivity towards a series of  $\alpha,\beta$ -unsaturated carbonyls and the results were listed in Table S4.

### Investigation of Active Sites in CoO<sub>x</sub>@CN for Hydrogenation of TMBQ

**Table 1.** Catalytic hydrogenation of TMBQ<sup>a</sup>

Entry	Catalysts	Conv. (%)	Yield (%)
1	CoO <sub>x</sub> @M	6	6
2	CoO <sub>x</sub> @G	6	6
3	CoO <sub>x</sub> @CN	92	92
4	CoO <sub>x</sub> @GL	60	60
5	CN	<1	<1
6	Co <sup>*</sup>	2	2
7 <sup>b</sup>	Co <sup>*</sup>	13	13
8	Co <sub>3</sub> O <sub>4</sub> <sup>*</sup>	<1	<1
9 <sup>b</sup>	Co <sub>3</sub> O <sub>4</sub> <sup>*</sup>	<1	<1
10	Co <sub>3</sub> O <sub>4</sub> /SiO <sub>2</sub>	<1	<1
11	Co <sub>3</sub> O <sub>4</sub> /ZrO <sub>2</sub>	<1	<1
12	Co <sub>3</sub> O <sub>4</sub> /TiO <sub>2</sub>	<1	<1
13	CoO <sub>x</sub> @CN-800	38	38
14	CoO <sub>x</sub> @CN-1000	50	50
15 <sup>c</sup>	AT-CoO <sub>x</sub> @CN <sup>1st</sup>	97	97
16 <sup>c</sup>	AT-CoO <sub>x</sub> @CN <sup>2nd</sup>	96	96
17 <sup>c</sup>	AT-CoO <sub>x</sub> @CN <sup>3rd</sup>	95	93

<sup>a</sup>Reaction conditions: 6.7 mmol TMBQ, 1.6 mol% Co to substrate, 15 mL i-propanol, 100 °C, 2 MPa H<sub>2</sub>, 6 h; <sup>b</sup>Reaction conditions are the same as <sup>a</sup>Reaction conditions except the reaction temperature is 120 °C; <sup>c</sup>Reaction conditions: 3.4 mmol TMBQ, 1.1 mol% Co to substrate, 7.5 mL i-propanol, 100 °C, 2 MPa H<sub>2</sub>, 6 h. \*Commercial metallic Co and Co<sub>3</sub>O<sub>4</sub> purchased from Aladdin, 5 mol% Co to substrate; All the results were determined by GC and GC-MS. The Co content of samples was summarized in Table S3.

Previous characterization verified that the CoO<sub>x</sub>@CN consists of nitrogen-doped carbon, Co<sub>3</sub>O<sub>4</sub> and metallic Co. The catalytic activity of CN (prepared without cobalt source) was firstly examined. As listed in Table 1, the CN showed negligible yield of TMHQ, demonstrating the nitrogen-doped carbon of the CoO<sub>x</sub>@CN is not responsible for the hydrogenation of TMBQ. Thus it is necessary to figure out whether Co<sub>3</sub>O<sub>4</sub> or the metallic Co is the real active site. Interestingly, the performance of commercial Co could be enhanced by increasing reaction temperature, although the yield is relatively low (Table 1, Entry 6-7). On the other hand, the activity of commercial Co<sub>3</sub>O<sub>4</sub> exhibited negligible yield even if the reaction temperature increases (Table 1, Entry 8-9). Further, supported Co<sub>3</sub>O<sub>4</sub> catalysts were also investigated the hydrogenation of TMBQ. The reaction results show that all the supported Co<sub>3</sub>O<sub>4</sub> catalysts obtain negligible yield (Table 1, Entry 10-12). XRD results show that the cobalt species existed in the phase of Co<sub>3</sub>O<sub>4</sub> before and after reaction (Fig. S5). No metallic Co was formed, implying that the phase of Co<sub>3</sub>O<sub>4</sub> did not turn into metallic Co during hydrogenation process. As a result, it is preliminarily deduced that metallic Co is the active sites.

Furthermore, materials with various metallic Co content were prepared to confirm the theory. Compared with CoO<sub>x</sub>@CN, the materials obtain at 800 °C and 1000 °C exhibit inferior catalytic behavior (Table 1, Entry 13-14). Detailed characterization was

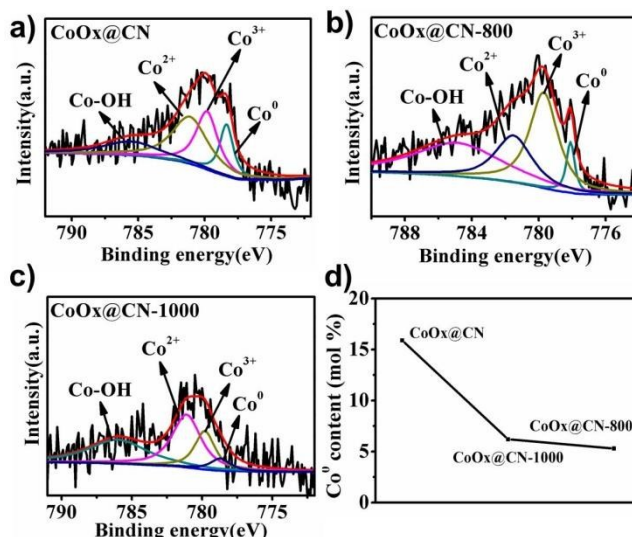


**Figure 3.** The patterns (a), (b), (c) are the high resolution of Co2p XPS spectra for the three samples; image (d) is the semiquantitative analysis of XPS.

carried out (Fig. S3 & S5). In terms of XRD characterization, all samples contain Co<sub>3</sub>O<sub>4</sub> and metallic Co. BET analysis demonstrates that all those three materials possess porous structure. Moreover, the specific surface area at 800 °C is even larger than the other two. However, a breakthrough was made in the analysis of high resolution of Co2p XPS spectra (Fig. 3). Although the typical XPS spectra of the three samples all verified the existence of metallic Co in the hybrid material,<sup>52,53</sup> the content of metallic Co in CoO<sub>x</sub>@CN was as almost three times as that of the other two samples according to the semiquantitative analysis. Thus, the metallic Co was deduced to be responsible for the hydrogenating of TMBQ. Furthermore, the material containing only metallic Co (named as AT-CoO<sub>x</sub>@CN) was obtained by treating CoO<sub>x</sub>@CN catalysts with 2M HCl solution (Fig. S6). In comparison to CoO<sub>x</sub>@CN, the AT-CoO<sub>x</sub>@CN catalyst gains higher yield even with lower cobalt content (Table 1, Entry 15-17), which reconfirms that metallic Co is the real active site. Besides, the catalyst could be reused for 3 times without significant activity degradation.

### Investigation of the Reaction Mechanism

The mechanism of the hydrogenation of TMBQ was investigated by using density functional theory (DFT) calculation from three parts (i).the adsorption of TMBQ on Co (1 1 1) surface (ii). hydrogenation of the first and second H adatoms to adsorbed TMBQ on Co (1 1 1) surface (iii).the competition between the desorption and the sequential hydrogenation of the products (TMBQ-2H).

Several adsorption configurations of TMBQ on the Co (1 1 1) surface were constructed and optimized. Geometry optimization results show the upright adsorption of TMBQ through O interacting with the surface is unstable, while the planar adsorption configurations through both C and O interacting with the surface are energetically favorable. These configurations that the benzoquinone ring adsorbs on the bridge and hollow sites of Co (1 1 1) surface almost in parallel with the surface are proved stable. The optimized stable

configurations are provided in Table S5 with the corresponding adsorption energies. The most stable configuration on Co (1 1 1) surface is shown in Figure 4 and will be used as the initial structure for further hydrogenation study. As shown in Figure 4, the length of the C-C bond was increased from 1.42 Å to 1.48 Å which is between the length of C-C single bond (1.34 Å) and C-C double bond (1.54 Å). The adsorbed atoms in TMBQ could be separated into four groups, O1 and C6, O2 and C3, C1 and C2, as well as C4 and C5, both adatoms in the same group sharing one corresponding surface metal atom in the  $\pi$ -bond mode. Even though the adsorption energy of TMBQ on Co (1 1 1) surface is -0.88 eV in the most stable configuration, we noted that all methyl and H groups at the benzoquinone ring tilt away from the surface. Considering the tilt might induce a quite high barrier in the adsorption process of TMBQ, we calculated the total energy along the adsorption path for TMBQ on Co (1 1 1) surface. As shown in Figure S7, when TMBQ closes to the metal surface gradually, there is an energy barrier of about 0.63 eV which could be reached easily in our experimental condition. Therefore, the most stable configuration we mentioned above could be used for further calculation.

After establishing the stable and available configuration of adsorbed TMBQ, the addition of the first and second hydrogen atoms to TMBQ was investigated. The major reaction steps are illustrated in Scheme 1. After the first hydrogen atom was added to different unsaturated atoms (C1, C2, C3, C4, C5, C6, O1 and O2), it is found that no stable configuration exists when C3 or C6 is first hydrogenated in that O1 and O2 mostly intend to bond to the surface. Regarding the energies of the stable configurations, those formed by hydrogenating C1 and C4 have the highest energies of 0.70 and 0.76 eV respectively, while those formed by hydrogenating O1, O2, C2 and C5 have the energies ranging only from 0.47 to 0.57 eV (Table S6). It suggests that thermodynamically O1, O2, C2 and C5 have a similar possibility to be hydrogenated. Then the initial energy and the activation barrier of adding the first hydrogen atom to the above four atoms were calculated respectively. Results show that the initial energy difference for positions mentioned above varies less than 0.1 eV. However, the activation barrier for the first hydrogen adding to O1 is as high as 0.86 eV,

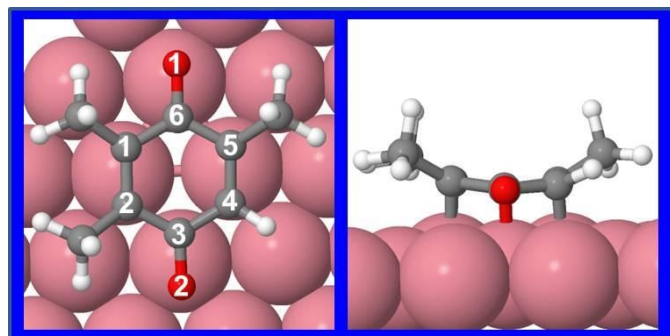
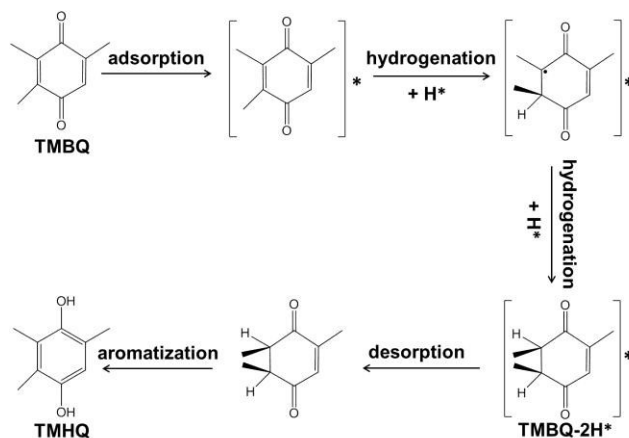


**Figure 4.** Top view (upper) and side view (lower) of TMBQ adsorption on Co (1 1 1) surface in the most stable configuration. Carbon atoms and oxygen atoms on benzoquinone ring are labeled. The Co atoms are in blue and the C, H, O atoms are in gray, white and red respectively.



**Scheme 1.** Major Reaction Pathway of TMBQ Hydrogenation on Co (1 1 1). The [ ]\* represents the adsorption states.

comparable to the highest excluded one (C4). Thereafter the most possible first hydrogenation positions are supposed to be C2, C5, and O2. The related structure during the hydrogenation can be seen in Figure S8. Then, we optimized the configuration after the second hydrogen was added (Table S7). It is found that sequential hydrogenation to C1 gives the lowest energy after C2 was hydrogenated first. Consequently, adding the first hydrogen atom to C2 was a favorable pathway compared to C5 and O2. Besides, in view of the sequential hydrogenation, the lower hydrogenation energy (0.76 eV) on C1 suggested the second H adatom is favored to be added to C1.

In consideration of the product, only two H were required to form TMHQ. However, the resulted intermediate was still adsorbed on the Co (1 1 1) surface after two Hs were hydrogenated. Therefore, the intermediate with two Hs already hydrogenated might undergo an over-hydrogenation process. Thus, the possibility of sequential hydrogenation of the third hydrogen adatom and desorption of TMBQ-2H was further investigated. The desorption energy of TMBQ-2H was 0.33 eV. As for the sequential hydrogenation, we compared the total energy after the third hydrogen atom was added to O1, O2, C4

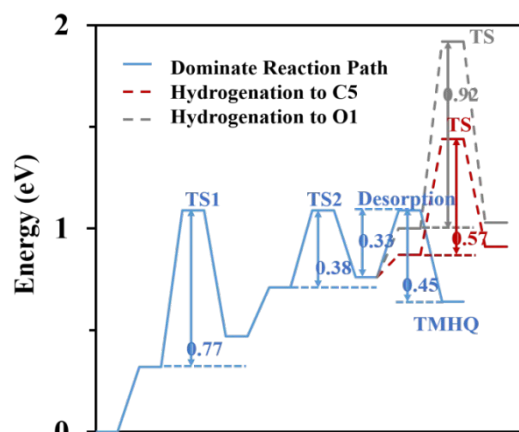


**Figure 5.** Potential energy profiles of TMBQ hydrogenation on Co (1 1 1) surface. Blue solid line indicates major reaction pathway, dashed grey and red lines are the addition of the third hydrogen adatom.

and C5. The results suggest that C5 and O1 might be sequentially hydrogenated. But the activation energies of both of them (C5 0.57 eV, O1 0.92 eV) are higher than the desorption energy (0.33 eV). In addition, the sequential hydrogenation process is an endothermic process which will increase the system energy (Figure 5). As a result, desorption of TMBQ-2H proceeds more easily than sequential hydrogenation, which is in line with our high selectivity (> 99%) to TMHQ.

#### Investigation of solvent effects.

Considering the solvent highly associated with catalytic activity, various solvents had been studied in the hydrogenation of TMBQ to TMHQ and the corresponding results were summarized in Table 2, along with the polarity of solvents. Among the solvents tested, dioxane provides the highest yield of 95 % with 100 % selectivity toward TMHQ, whereas toluene and cyclohexane give an unexpected conversion. Although the mechanism of the solvent impact on the heterogeneous catalysis is not clear, some conclusions could be rationalized by correlating the reaction rate and selectivity with solvent polarity. According to the analysis of the reaction results in our system, it is easy to conclude that the solvent polarity plays an important part in determining the TMBQ conversion, but does not affect the selectivity toward TMHQ significantly. The influence of protic solvent on such reaction was also investigated. The comparison of Entries 1,4,5 with Entries 2,3 in Table 2 indicated no significant difference between protic solvents and aprotic solvents. It is worthy of note that high yield is achieved with water, though TMBQ is not soluble in water, which might be explained by the enhancement of hydrophilic property resulting from the N-doping in the carbon matrix, improving the catalyst dispersion in water and the exposure of the catalyst to the substrate, thereby increasing the catalytic performance.<sup>54,55</sup>

**Table 2.** Hydrogenation of TMBQ over CoO<sub>x</sub>@CN in various solvents<sup>a</sup>

Entry	Solvent	Conv.(%)	Yield(%)	Polarity
1	Water	91	91	10.2
2	Acetone	93	93	5.4
3	Dioxane	95	95	4.8
4	i-Propanol	92	92	4.3
5	Ethanol	84	84	4.3
6	Ethyl acetate	44	44	4.3
7	Toluene	30	30	2.4
8	Cyclohexane	3	3	0.1

<sup>a</sup>Reaction conditions: 6.7 mmol TMBQ, 1.6 mol% Co to substrate, 15 mL solvent, 120°C, 3 MPa H<sub>2</sub>, 6 h. All the results were determined by GC and GC-MS.

#### Conclusions

In summary, we successfully developed a novel method to fabricate uniform cobalt-based NPs supported on porous, nitrogen-doped carbon. The as-prepared catalyst showed high yield (> 90 %) and selectivity (> 99 %) for hydrogenation of TMBQ as well as  $\alpha$ ,  $\beta$ -unsaturated carbonyls. The metallic Co

was proved to be the active site for hydrogenating TMBQ. DFT calculations revealed that TMBQ was adsorbed on Co with the benzoquinone ring almost in parallel with the surfaces. The first and second hydrogen atoms were added to the C2-C1 double bond sequentially. The excellent chemoselectivity to TMHQ was assigned to the favorable desorption process rather than sequential hydrogenation of TMHQ on the CoO<sub>x</sub>@CN catalyst. The effect of solvent was also investigated, indicating that the activity increased with solvent polarity while selectivity almost had nothing to do with polarity. The present work did not only report a novel material for TMBQ hydrogenation, but also initiated a new academic direction to study the mechanism of TMBQ hydrogenation.

#### Acknowledgement

Financial support from the National Natural Science Foundation of China (91534114 & 21376208), the Zhejiang Provincial Natural Science Foundation for Distinguished Young Scholars of China (LR13B030001), the Specialized Research Fund for the Doctoral Program of Higher Education (J20130060), the Fundamental Research Funds for the Central Universities, the Program for Zhejiang Leading Team of S&T Innovation, and the Partner Group Program of the Zhejiang University and the Max-Planck Society are greatly appreciated.

#### Notes and references

- L. L. Adduci, T. A. Bender, J. A. Dabrowski and M. R. Gagné, *Nat. Chem.*, 2015, **7**, 576-581.
- P. Mäki-Arvela, J. Hájek, T. Salmi and D. Y. Murzin, *Appl. Catal. A*, 2005, **292**, 1-49.
- H.-U. Blaser, C. Malan, B. Pugin, F. Spindler, H. Steiner and M. Studer, *Adv. Synth. Catal.*, 2003, **345**, 103-151.
- M. J. Climent, A. Corma, P. De Frutos, S. Iborra, M. Noy, A. Velty and P. Concepción, *J. Catal.*, 2010, **269**, 140-149.
- S. Vernuccio, P. R. von Rohr and J. Medlock, *Ind. Eng. Chem. Res.*, 2015, **54**, 11543-11551.
- C. Li, X. Zhao, A. Wang, G. W. Huber and T. Zhang, *Chem. Rev.*, 2015, **115**, 11559-11624.
- R. Schlögl, *Angew. Chem. Int. Ed.*, 2015, **54**, 3465-3520.
- C. Zhao, J. He, A. A. Lemonidou, X. Li and J. A. Lercher, *J. Catal.*, 2011, **280**, 8-16.
- T. Yuan, H. Gong, K. Kailasam, Y. Zhao, A. Thomas and J. Zhu, *J. Catal.*, 2015, **326**, 38-42.
- J. Yang, S. Li, N. Li, W. Wang, A. Wang, T. Zhang, Y. Cong, X. Wang and G. W. Huber, *Ind. Eng. Chem. Res.*, 2015, **54**, 11825-11837.
- Z. Shao, C. Li, X. Di, Z. Xiao and C. Liang, *Ind. Eng. Chem. Res.*, 2014, **53**, 9638-9645.
- M. Carril, P. Altmann, M. Drees, W. Bonrath, T. Netscher, J. Schütz and F. E. Kühn, *J. Catal.*, 2011, **283**, 55-67.
- W. Bonrath, M. Eggersdorfer and T. Netscher, *Catal. Today*, 2007, **121**, 45-57.
- F. Jung, US2259936[P], 1941-1901-1921.
- S. Mukhopadhyay, K. H. Chandnani and S. B. Chandalia, *Org. Process Res. Dev.*, 2000, **4**, 254-258.
- X. Zhao, Y. Jin, F. Zhang, Y. Zhong and W. Zhu, *Chem. En. J.*, 2014, **239**, 33-41.
- T. Zhang, G. Yin, B. Li, X. Wang, S. Jiang and Z. Yuan, *Res. Chem. Intermed.*, 2015, **41**, 663-677.

- 18 R. V. Jagadeesh, A.-E. Surkus, H. Junge, M.-M. Pohl, J. Radnik, J. Rabeah, H. Huan, V. Schünemann, A. Brückner and M. Beller, *Science*, 2013, **342**, 1073-1076.
- 19 F. A. Westerhaus, R. V. Jagadeesh, G. Wienhöfer, M.-M. Pohl, J. Radnik, A.-E. Surkus, J. Rabeah, K. Junge, H. Junge, M. Nielsen, A. Brückner and M. Beller, *Nat. Chem.*, 2013, **5**, 537-543.
- 20 T. Stemmler, F. A. Westerhaus, A.-E. Surkus, M.-M. Pohl, K. Junge and M. Beller, *Green Chem.*, 2014, **16**, 4535-4540.
- 21 Ø. Borg, P. D. C. Dietzel, A. I. Spjelkavik, E. Z. Tveten, J. C. Walmsley, S. Diplas, S. Eri, A. Holmen and E. Rytter, *J. Catal.*, 2008, **259**, 161-164.
- 22 A. K. Dalai and B. H. Davis, *Appl. Catal. A*, 2008, **348**, 1-15.
- 23 M. T. Reetz and K. Töllner, *Tetrahedron Lett.*, 1995, **36**, 9461-9464.
- 24 Z. Wei, J. Wang, S. Mao, D. Su, H. Jin, Y. Wang, F. Xu, H. Li and Y. Wang, *ACS Catal.*, 2015, 4783-4789.
- 25 H. Wang, K. An, A. Sapi, F. Liu and G. Somorjai, *Catal. Lett.*, 2014, **144**, 1930-1938.
- 26 P. Serna and B. C. Gates, *Accounts. Chem. Res.*, 2014, **47**, 2612-2620.
- 27 R. J. White, R. Luque, V. L. Budarin, J. H. Clark and D. J. Macquarrie, *Chem. Soc. Rev.*, 2009, **38**, 481-494.
- 28 P. Zhang, J. Yuan, T.-P. Fellinger, M. Antonietti, H. Li and Y. Wang, *Angew. Chem. Int. Ed.*, 2013, **125**, 6144-6148.
- 29 X. Xu, Y. Li, Y. Gong, P. Zhang, H. Li and Y. Wang, *J. Am. Chem. Soc.*, 2012, **134**, 16987-16990.
- 30 Z. Li, J. Liu, Z. Huang, Y. Yang, C. Xia and F. Li, *ACS Catal.*, 2013, **3**, 839-845.
- 31 Z. Wei, Y. Gong, T. Xiong, P. Zhang, H. Li and Y. Wang, *Catal. Sci. Technol.*, 2015, **5**, 397-404.
- 32 Y. Liang, H. Wang, P. Diao, W. Chang, G. Hong, Y. Li, M. Gong, L. Xie, J. Zhou, J. Wang, T. Z. Regier, F. Wei and H. Dai, *J. Am. Chem. Soc.*, 2012, **134**, 15849-15857.
- 33 Y. Liu, H. Dai, J. Deng, S. Xie, H. Yang, W. Tan, W. Han, Y. Jiang and G. Guo, *J. Catal.*, 2014, **309**, 408-418.
- 34 H. Zhang, H. Li, X. Li, H. Qiu, X. Yuan, B. Zhao, Z.-F. Ma and J. Yang, *Int. J. Hydrogen. Energy*, 2014, **39**, 267-276.
- 35 K.-Y. Andrew Lin, F.-K. Hsu and W.-D. Lee, *J. Mater. Chem. A*, 2015, **3**, 9480-9490.
- 36 Y. Yoon, R. Rousseau, R. S. Weber, D. Mei and J. A. Lercher, *J. Am. Chem. Soc.*, 2014, **136**, 10287-10298.
- 37 G. Li, J. Han, H. Wang, X. Zhu and Q. Ge, *ACS Catal.*, 2015, **5**, 2009-2016.
- 38 G. Kresse and J. Furthmüller, *Comp. Mater. Sci.*, 1996, **6**, 15-50.
- 39 G. Kresse and J. Furthmüller, *Phys. Rev. B*, 1996, **54**, 11169-11186.
- 40 P. E. Blöchl, *Phys. Rev. B*, 1994, **50**, 17953-17979.
- 41 G. Kresse and D. Joubert, *Phys. Rev. B*, 1999, **59**, 1758-1775.
- 42 B. Hammer, L. B. Hansen and J. K. Nørskov, *Phys. Rev. B*, 1999, **59**, 7413-7421.
- 43 G. Henkelman, B. P. Uberuaga and H. Jónsson, *J. Chem. Phys.*, 2000, **113**, 9901-9904.
- 44 J. Wang, Z. Xu, Y. Gong, C. Han, H. Li and Y. Wang, *ChemCatChem*, 2014, **6**, 1204-1209.
- 45 R. Nie, J. Shi, W. Du, W. Ning, Z. Hou and F.-S. Xiao, *J. Mater. Chem. A*, 2013, **1**, 9037-9045.
- 46 J. E. Spanier, R. D. Robinson, F. Zhang, S.-W. Chan and I. P. Herman, *Phys. Rev. B*, 2001, **64**, 245407.
- 47 V. Chandra, J. Park, Y. Chun, J. W. Lee, I.-C. Hwang and K. S. Kim, *ACS Nano*, 2010, **4**, 3979-3986.
- 48 Y. Gong, P. Zhang, X. Xu, Y. Li, H. Li and Y. Wang, *J. Catal.*, 2013, **297**, 272-280.
- 49 S. Kubo, R. J. White, N. Yoshizawa, M. Antonietti and M. M. Titirici, *Chem. Mater*, 2011, **23**, 4882-4885.
- 50 H. Jin, J. Wang, D. Su, Z. Wei, Z. Pang and Y. Wang, *J. Am. Chem. Soc.*, 2015, **137**, 2688-2694.
- 51 M. Tang, S. Mao, M. Li, Z. Wei, F. Xu, H. Li and Y. Wang, *ACS Catal.*, 2015, **5**, 3100-3107.
- 52 J. Zhu, K. Kailasam, A. Fischer and A. Thomas, *ACS Catal.*, 2011, **1**, 342-347.
- 53 S. C. Petitto and M. A. Langell, *J. Vac. Sci. Technol. A*, 2004, **22**, 1690-1696.
- 54 H. Wan, A. Vitter, R. V. Chaudhari and B. Subramaniam, *J. Catal.*, 2014, **309**, 174-184.
- 55 J. He, C. Zhao and J. A. Lercher, *J. Catal.*, 2014, **309**, 362-375.

**Graphical Abstract:**

We successfully developed a one-pot method to synthesize Co-based catalysts (denoted as  $\text{CoO}_x@\text{CN}$ ), showing high activity and selectivity for TMBQ hydrogenation along with  $\alpha$ ,  $\beta$ -unsaturated carbonyls. The metallic Co was proved to be the real active site for hydrogenation and the hydrogenation process was also investigated by DFT calculation on Co (1 1 1) surface.

